PRIFYSGOL BANGOR / BANGOR UNIVERSITY

PRIFYSGOL BANGOR UNIVERSITY

Hybrid OFDM-Digital Filter Multiple Access PONs Utilizing Spectrally Overlapped Digital Orthogonal Filtering

Sankoh, Abdulai; Jin, Wei; Zhong, Zhuqiang; He, Jiaxiang; Hong, Yanhua; Giddings, Roger; Pierce, Ian; O'Sullivan, Maurice; Lee, Jeffrey; Durrant, Tim; Tang, Jianming

IEEE Photonics Journal

Peer reviewed version

Cyswllt i'r cyhoeddiad / Link to publication

01. Jun. 2021

Hybrid OFDM-Digital Filter Multiple Access PONs Utilizing Spectrally Overlapped Digital Orthogonal Filtering

A. Sankoh,[1] W. Jin,[1] Z. Q. Zhong,[1] J. X. He,[1] Y. H. Hong,[1] R. P. Giddings,[1] *Member, IEEE,*
I. Pierce,[1] M. O'Sullivan,[2] J. Lee,[3] T. Durrant,[3] and J. M. Tang[1] *Member, IEEE*

[1]School of Computer Science and Electronic Engineering, Bangor University, Bangor, LL57 1UT, U.K.
[2]Ciena Canada, Inc., 385 Terry Fox Drive, Ottawa, Ontario K2K 0L1, Canada.
[3]EFFECT Photonics LTD. Brixham Laboratory, Freshwater Quarry, Brixham, Devon, England, TQ5 8BA, UK.

Abstract: Known hybrid orthogonal frequency division multiplexing-digital filter multiple access (OFDM-DFMA) PONs show promise of seamless and cost-effective convergence of optical and mobile networks for 5G and beyond. This paper reports, for the first time, a new hybrid OFDM-DFMA PON based on intensity modulation and direct detection (IMDD), obtained by modifying digital signal processing (DSP) algorithms embedded in both the OLT and ONUs. The proposed PON allows two spectrally overlapped sub-bands to occupy each individual sub-wavelength spectral region to independently transmit upstream ONU information. A model of the proposed PON is developed and its upstream transmission performances are numerically explored for different application scenarios. Compared with the previously published PON, the proposed PON doubles the number of supported ONUs and provides >1.7-fold aggregate upstream signal transmission capacity increases with <1.5dB upstream power budget degradations. Alternately, for the same ONU count, >2.2-fold aggregate upstream signal transmission capacity increases and >0.7dB upstream power budget improvements are achievable. The performance improvements vary by <18% for a transmission distance range as large as 50km. In addition, the proposed PON is tolerant to finite digital filter tap length-induced channel interferences.

Index Terms: Digital filter multiple access (DFMA), intensity modulation and direct detection (IMDD), orthogonal frequency division multiplexing (OFDM), digital signal processing (DSP) and passive optical network (PON).

1. Introduction

The evolution and accelerating increase in the number of smart mobile devices, stoked by new content-rich services and highly dynamic on-demand bandwidth-hungry video-centric mobile services [1], [2], have made cloud radio access networks (C-RANs) a key enabler for 5G and beyond networks [3]. A 5G C-RAN architecture mainly includes three types of network connections, namely, mobile front-haul (MFH), mobile mid-haul (MMH) and mobile back-haul (MBH). The MFH connects a remote radio unit (RRU) and a distributed unit (DU), while the MMH connects the DU and a central unit (CU), and the MBH connects the CU and a 5G core network (5GC). Practical, cost effective high-speed 5G C-RANs can be based on intensity modulation and direct detection in a passive optical network (IMDD PON) [4], [5]. However, some modifications to existing IMDD PONs are required to deliver high data rate, low latency and ubiquitous access [6]-[8], and address surging dynamic mobile traffic. Furthermore, it is desirable to equip the PONs with software-defined networking (SDN) and network function virtualization (NFV) across all the network layers for more efficient network operation and resource utilization. Finally, to reduce network cost, the PONs should enable convergence of existing optical metropolitan, optical access, and mobile networks.

A digital filter multiple access (DFMA) PON based on IMDD has been proposed to address these requirements [9]. It uses SDN-controllable digital orthogonal filters in each optical network unit (ONU) and optical line terminal (OLT) to dynamically multiplex/demultiplex many spectrally overlapped sub-bands of arbitrary bandwidth granularity. This does not require extra analogue hardware compared to conventional PON transceivers. Extensive numerical investigations and experimental demonstrations of the IMDD DFMA PONs have been reported in [9]-[13]. However, as the number of required digital matching filters embedded in the OLT is proportional to the overall channel count, for a large number of ONUs, the OLT digital signal processing (DSP) complexity grows uncomfortably large for cost-sensitive mobile applications. A comparatively low DSP complexity IMDD PON with inherent transparency to 4G mobile networks, termed hybrid
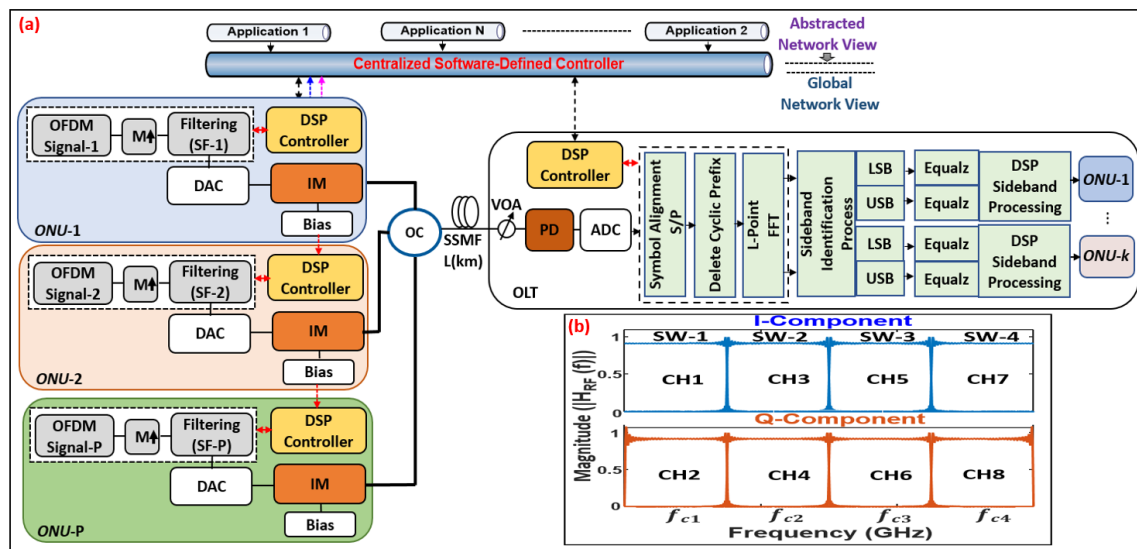
Fig. 1 (a) Schematic diagram of orthogonal digital filtering-based hybrid OFDM-DFMA PON based on IMDD (b) frequency responses of the orthogonal digital shaping filters implemented in ONUs. M↑: digital up-sampling factor, SF: shaping filter, DAC/ADC: digital-to-analogue/analogue-to-digital converter. IM: intensity modulator. OC: optical coupler, PD: photo diode. S/P: serial-to-parallel conversion, LSB: lower sideband, USB: upper sideband, Equalz: equalization, ONU: optical network unit, DSP: digital signal processing, OLT: optical line terminal, SW: sub-wavelength, CH: channel.

orthogonal frequency division multiplexing (OFDM)-DFMA PON, has been proposed and investigated [14]. For upstream transmission, this PON applies an ONU DSP procedure similar to the DFMA-PON, i.e., each ONU uses its embedded digital in-phase (referred to as I-phase throughout the paper) shaping filter to locate its OFDM signal at an assigned radio frequency spectral region (referred to as sub- wavelength throughout the paper). Whilst in the OLT, a single fast Fourier transform (FFT) operation and relevant DSP processes are pipelined to simultaneously demultiplex and demodulate the received OFDM signals from different ONUs without using any digital matching filters (MFs). Compared to the DFMA PON, the hybrid OFDM-DFMA PON reduces the OLT DSP complexity by a factor of >100 when ONU counts are ≥ 32. This can also lower transceiver cost and power consumption. More importantly, the hybrid OFDM-DFMA PON provides upstream performance tolerance to transceiver sample timing offset, channel interferences, digital filter characteristic variations and transmission system nonlinearity impairments, due to the MF-free receiver DSP design in the OLT [14]. Consequently, >10dB upstream ONU error vector magnitude (EVM) performance improvements provided sufficient received optical powers, and 16dB increases in differential ONU launch power dynamic range are achievable [14]. However, in contrast to the DFMA PON which supports simultaneously two spectrally overlapped sub-bands at each sub-wavelength, the hybrid OFDM-DFMA PON can only transmit a single upstream double sideband (DSB) OFDM signal in any sub-wavelength spectral region. As such, compared to the DFMA PON, the hybrid OFDM-DFMA PON has half of the aggregate signal transmission capacity and overall spectral efficiency.

In this paper, we show that spectral efficiency can be reclaimed with a new variant of the hybrid OFDM-DFMA PON, in which the DSP algorithms embedded in both the OLT and ONUs are slightly modified to allow two spectrally overlapped sub-bands to occupy each individual sub-wavelength for independent upstream transmission of ONU information. In particular, for the proposed PON, each ONU utilizes a DSP procedure identical to the DFMA PON to produce one or two orthogonal OFDM sub-band(s) occupying the same or different sub-wavelength(s) [9]. In the OLT, similar to the previously reported hybrid OFDM-DFMA PON, a single FFT operation is applied and an operation is conducted to identify the subcarriers in the lower and upper sidebands (LSB and USB, respectively) of each sub-band. After pilot-aided channel estimation and equalization for the LSB and USB, the two received spectrally overlapped OFDM sub-bands of a single sub-wavelength are finally demultiplexed by summing and subtracting the LSB and USB subcarriers of the sub-wavelength. Since the OLT in the proposed PON is still free from digital MFs and uses a pipelined approach in demodulating all received spectrally overlapped OFDM sub-bands, it follows that, compared to earlier reported hybrid OFDM-DFMA PONs, this PON has higher (nearly double) signal transmission capacity and spectral efficiency. It also retains the

properties of earlier hybrid OFDM-DFMA PONs, namely, lower OLT DSP complexity, inherent transparency to 4G networks and performance robustness to physical-layer network design factors such as digital filter variations, channel crosstalk and transmission impairments as well as transceiver sample timing offset.

In this paper, we present a model of the proposed PON and numerically explore its upstream transmission performances for various application scenarios. Our results show that compared with previously reported PON, the proposed PON supports twice the number of passively multiplexed ONUs, and a >1.7-fold aggregate upstream signal transmission capacity increase is obtained with <1.5dB upstream power budget degradations. Alternately, when the proposed PON supports the same number of ONUs each occupying two digitally multiplexed orthogonal sub-bands, a >2.2-fold aggregate upstream signal transmission capacity increase and a >0.7dB upstream power budget improvement can be achieved. For a transmission distance range as large as large as 50km, these performance improvements vary by <18% and are robust to finite digital filter tap-induced channel interferences. The aforementioned performances of the proposed PON are similar to those of a recently published PON termed hybrid single sideband OFDM-DFMA PON [15], whose ONU DSP complexity is, however, significantly higher than the proposed PON.

2. Operating Principle and Theoretical Model

The schematic diagram of the proposed new hybrid OFDM-DFMA PON based on IMDD is shown in Fig. 1(a) for upstream transmission only. As shown in Fig. 1(a), passively coupled upstream optical signals from P ONUs labelled as ONU1, ONU2…, ONUP are generated using pairs of different digital orthogonal shaping filters. Signals are processed in each ONU using a DSP procedure similar to that of [14]. This includes DSP algorithms for real-valued OFDM signal generation, M× digital domain up-sampling and digital filtering. To simplify the theoretical analyses, ideal digital filter responses are assumed in this section only. The I-phase sub-band occupies the i-th sub-wavelength, as illustrated in Fig. 1(b), and can be expressed as:

$$S_i^I(t) = \sum_{k=-N/2}^{N/2-1} \left[a_{k,i} e^{j2\pi k \left(\frac{f_{DAC/ADC}}{MN} \right) t} \right] e^{j2\pi f_{ci} t} + \tag{1}$$

$$\sum_{k=-N/2}^{N/2-1} \left[a_{k,i}^* e^{-j2\pi k \left(\frac{f_{DAC/ADC}}{MN} \right) t} \right] e^{-j2\pi f_{ci} t}$$

where $a_{k,i}$ is the encoded data conveyed on the k-th subcarrier of the i-th sub-wavelength. $f_{ci} = ((2 \times i - 1) \times f_{DAC/ADC} / 2M)$ is the sub-wavelength center frequency, where $f_{DAC/ADC}$ is the sampling rates of the digital-to-analog/analog-to-digital converter (DAC/ADC). N is the IFFT size used in generating the OFDM signal. * is the conjugation operator. In Eq. (1), the first term represents the total number of N OFDM subcarriers located at the positive frequency bin in the i-th sub-wavelength spectral region, while the second term represents their counterpart in the negative frequency bin. Among these N OFDM subcarriers in the positive frequency bin, there are $N/2$ LSB subcarriers, which are the conjugation of the remaining $N/2$ USB subcarriers, i.e. $a_{-m,i} = a_{m,i}^*$, $m = 1,2,…(N/2-1)$ and $a_0 = a_{-N/2} = 0$ [14].

In similarity with Eq.(1), when an ONU employs the Q-phase digital shaping filter to locate its OFDM signal which occupies the i-th sub-wavelength as illustrated in Fig. 1(b), the digitally filtered OFDM signal can be written as:

$$S_i^Q(t) = \sum_{k=-N/2}^{N/2-1} \left(\left[b_{k,i} e^{j2\pi k \left(\frac{f_{DAC/ADC}}{MN} \right) t} \right] e^{j2\pi f_{ci} t} \right) \times (-j) + \tag{2}$$

$$\sum_{k=-N/2}^{N/2-1} \left(\left[b_{k,i}^* e^{-j2\pi k \left(\frac{f_{DAC/ADC}}{MN} \right) t} \right] e^{-j2\pi f_{ci} t} \right) \times (j)$$

where $b_{k,i}$ is the encoded data conveyed on the k-th subcarrier of the i-th sub-wavelength.
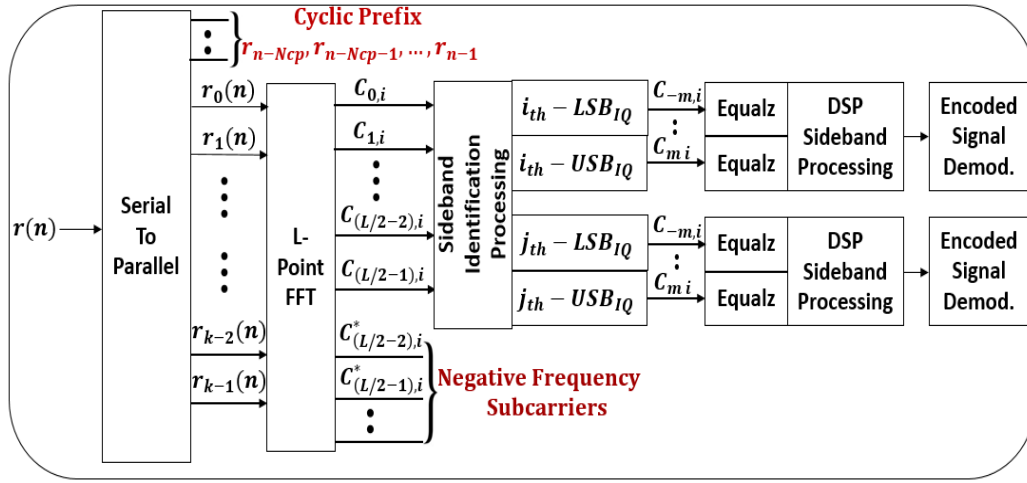
Fig. 2 Block diagram of OLT DSP procedure of the proposed PON.

Comparing Eq. (1) and Eq. (2), it can be seen that after digital filtering processing, the Q-phase OFDM subcarriers in the positive frequency bin have a -π/2 phase rotation when compared to the corresponding I-phase OFDM subcarriers. The phase rotation is caused by the Q-phase digital shaping filters.

After the DAC, optical intensity modulation converts the electrical signal to an optical signal. For the i-th ONU, the produced optical signal can be given by:

$$S_{opt-i}(t) = \left[\beta_i(t)e^{j\alpha_i(t)} \cdot \sqrt{1 + \zeta_i * S_i^W(t)}\right]e^{j2\pi f_{opt}t}, \quad w = I \ or \ Q \quad (3)$$

where f_{opt} is the center frequency of the optical signal. ζ_i is the intensity modulation index. $\beta_i(t)$ and $\alpha_i(t)$ stand for the optical intensity modulation-induced optical amplitude and phase of the optical signal $S_{opt-i}(t)$. When $w=I$, the optical signal contains an I-phase OFDM sub-band, while for $w=Q$, it consists of a Q-phase sub-band. Without losing generality, here both the I-phase sub-band and the Q-phase sub-band are assumed to be at a single sub-wavelength.

For upstream transmission, in the remote node, a total number of P optical signals from various ONUs are passively combined to produce a signal waveform that can be written as:

$$S_{opt}(t) = \sum_{i=1}^{P}\left[\beta_i(t)e^{j\alpha_i(t)} \cdot \sqrt{1 + \zeta_i * S_i^W(t)}\right]e^{j2\pi f_{opt}t} \quad (4)$$

After upstream transmission, in the OLT, by excluding noise and optical transmission effects and following optical-electrical (O-E) conversion and an ADC, the received signal S_{IQ}, comprise of multiple pairs of orthogonal sub-bands in different sub-wavelengths. Assuming that the overall sub-wavelength number is U and each subwavelength conveys two independent orthogonal OFDM sub-bands, we have $2U=P$, and S_{IQ} can be expressed as:

$$S_{IQ} = \sum_{i=1}^{U}\left\{S_i^I(t) + S_i^Q(t)\right\}$$

$$= \sum_{i=1}^{U}\left\{\left(\sum_{k=-N/2}^{N/2-1} c_{k,i}e^{j2\pi k\left(\frac{f_{DAC/ADC}}{MN}\right)t}\right)e^{j2\pi f_{ci}t} + \right.$$

$$\left.\left(\sum_{k=-N/2}^{N/2-1} c_{k,i}^* e^{-j2\pi k\left(\frac{f_{DAC/ADC}}{MN}\right)t}\right)e^{-j2\pi f_{ci}t}\right\} \quad (5)$$

Where $c_{k,i}$ is the received data from the k-th subcarrier in the i-th sub-wavelength. In Eq. (5), the first term is all the subcarriers in the positive frequency bin, while the second is their counterparts in the negative frequency bin. As seen in Fig. 2, in the OLT, after serial-to-parallel (S/P) conversion and cyclic prefix (CP) removal, an L-point FFT operation is applied with L satisfying $L=2UN$. After that, the $L/2$ subcarriers in the positive frequency bin are classified into U groups each consisting of N subcarriers. Here the N subcarriers in the i-th group occupy the i-th sub-wavelength. The group's $N/2$ low frequency subcarriers occupy the LSB of the sub-band, and the remaining $N/2$ high frequency subcarriers occupy the USB of the same sub-band. The received subcarrier matrix of the i-th sub-wavelength can then be described as:

$$C_i = \left[\overbrace{c_{-N/2,i}, c_{-N/2+1,i}, \cdots\cdots\cdots, c_{-1,i}}^{LSB}, \underbrace{c_{0,i}, c_{1,i}, \cdots\cdots\cdots c_{-1+N/2,i}}_{USB} \right] \tag{6}$$

In addition, it should also be noted that the subcarrier matrix C_i, is the sum of the received I-phase sub-band subcarriers and Q-phase sub-band subcarriers. Under an assumption of a linear transmission system and considering Eq. (1) and Eq. (2), Eq. (6) can be rewritten as:

$$C_i = \left[\begin{array}{l} \overbrace{(a_{-N/2,i} - jb_{-N/2,i}), \ldots, (a_{-1,i} - jb_{-1,i})}^{LSB}, \\ \underbrace{(a_{0,i} - jb_{0,i}), \cdots\cdots, (a_{-1+N/2,i} - jb_{-1+N/2,i})}_{USB} \end{array} \right] \tag{7}$$

Because of $a_{-m,i}=a^*_{m,i}$ and $b_{-m,i}=b^*_{m,i}$, $m=1,2,\ldots(N/2-1)$, we can have;

$$c_{-m,i} = a_{-m,i} - jb_{-m,i} = a^*_{m,i} - jb^*_{m,i} \tag{8}$$

$$c_{m,i} = a_{m,i} - jb_{m,i} \tag{9}$$

Here $c_{-m,i}$ and $c_{m,i}$ represent the subcarriers in the LSB and USB of the orthogonal sub-bands occupying the i-th sub-wavelength. To demultiplex the spectrally overlapped data $a_{m,i}$ and $b_{m,i}$, Eq. (8) and Eq. (9) can be rewritten as:

$$a_{m,i} = \frac{1}{2}\left[c^*_{-m,i} + c_{m,i}\right],$$

$$b_{m,i} = \frac{1}{j2}\left[c^*_{-m,i} - c_{m,i}\right] \tag{10}$$

Based on Eq. (10), it can be seen that in the OLT, orthogonal sub-bands for each sub-wavelength can be demultiplexed. A conjugation operation is applied to the received LSB subcarriers, then sum and subtraction operations are carried out between these subcarriers in the LSB and USB of the same sub-wavelength. In practice, the received LSB and USB subcarriers of the same sub-wavelength may suffer different signal distortions due to transmission system nonlinearities. To minimize this distortion, the LSB and USB subcarriers in each sub-wavelength undergo independent pilot-aided channel estimation and equalization [16] prior to summation and subtraction. For the LSB subcarrier equalization, the received LSB pilot subcarriers are the sum of the I-phase sub-band pilot subcarriers and (+j)-multiplied Q-phase sub-band pilot-subcarriers. On the other hand, for the USB subcarrier equalization, the received USB pilot subcarriers are the sum of the conjugate I-phase sub-band pilot subcarriers and (-j)-multiplied conjugate Q-phase sub-band pilot-subcarriers.

TABLE 1
TRANSCEIVER PARAMETERS

Parameter	Value	Parameter	Value
DAC/ADC Sample Rate	30GS/s	DAC/ADC effective number of bits	8-bits
OFDM IFFT/FFT Size	32/256	Clipping Ratio (Hybrid Case-I / Hybrid Case-IIA / Hybrid Case-IIB)	11dB / 10dB / 9dB
Number of Data Carrying Subcarriers	15	Digital Filter Length	64
Modulation Format	16-QAM	Excess of the Bandwidth	0
Number of Transmitted Symbols	6000	PIN Detector Quantum Efficiency	0.8 A/W
Training Symbols	50	PIN Detector Sensitivity	-19 dBm
Cyclic Prefix	12.5%	PIN Detector Bandwidth	Ideal
Channel Bitrate	6.25Gb/s	Fiber Dispersion Slope	0.08 ps/nm²/km
Optical Launch Power	0 dBm	Fiber Loss	0.2 dB/km
Up-sampling Factor(M)	8	Fiber Kerr Coefficient	2.6×10^{-20} m²/W
FEC overhead	~7%	Transmission distance	40km

*Corresponding to 10 Gb/s non-return-to-zero data at a BER of 1.0×10^{-9}

3. Numerical Simulation conditions

To verify the model developed in Section 2 for use in practical nonlinear IMDD PON scenarios, in this Section we calculate its upstream transmission performance over 40km standard single mode fiber (SSMF). Optical fiber transmissions are simulated using VPItransmissionMaker. Upstream performance comparisons are also made between the proposed PON and the previously reported PON [14] (used as a reference). Each PON has four identical sub-wavelength regions, as
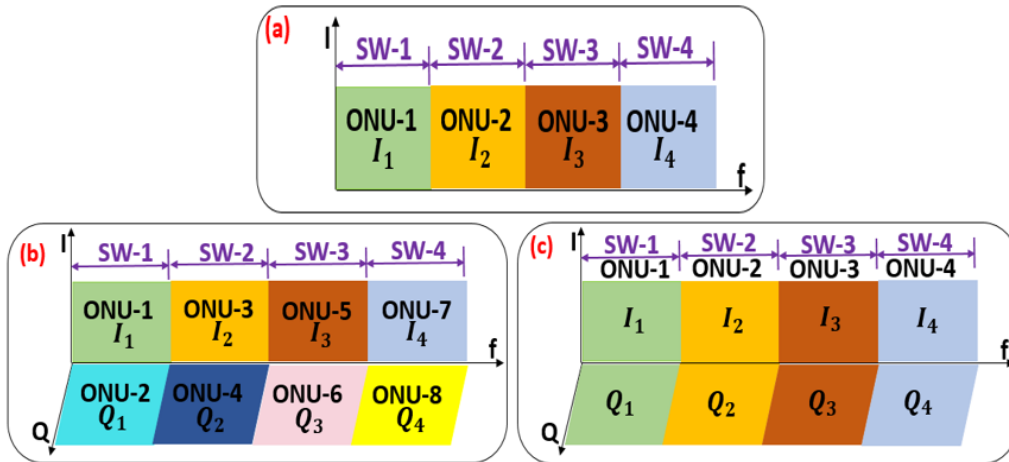

Fig. 3 Spectral locations of the digitally filtered signals in different sub-wavelength spectral region. (a) Hybrid Case-I (b) Hybrid Case-IIA and (c) Hybrid Case-IIB. SW: sub-wavelength, ONU: optical network unit, I: in-phase, Q: quadrature-phase.

illustrated in Fig. 3. The PON of [14], labeled Hybrid Case-I, contains four 4 ONUs each occupying an I-phase OFDM sub-band in a single sub-wavelength. The proposed PON occupies the same bandwidth and has two cases: Hybrid Case-II(A) and Hybrid Case-II(B). Hybrid Case-II(A) contains eight ONUs each occupying a single sub-band and sharing a sub-wavelength with another ONU. Hybrid Case-II(B) involves four ONUs, each of which produces an optical signal comprising two orthogonal sub-bands that share a single sub-wavelength. MATLAB is used to perform signal generations and digital filtering.

Fig. 1(a) illustrates the simulation setup for evaluating upstream transmission performances of the two PONs. For the three cases described above, the parameters listed in Table I are used to generate real-valued OFDM signals and required digital filters. In Hybrid Case-I, four orthogonal
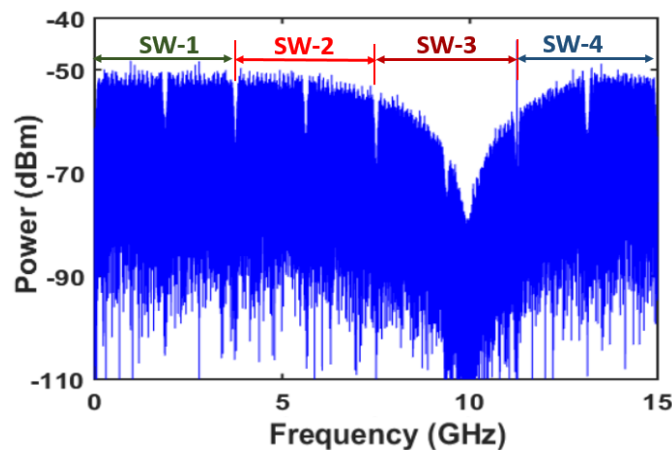
Fig. 4. Signal spectrum after 40km fiber transmission over SSMF link. An ideal PIN with an unlimited bandwidth is considered.

digital filter pairs are produced and only the I-phase digital filters are used, while for Hybrid Case-II(A) and Hybrid Case-II(B), both the I-phase and Q-phase digital filters are employed. The spectral locations of the digital filtered OFDM sub-bands for all three cases are shown in Fig. 3. The approach reported in [15], [17] are used to determine optimum clipping ratios for the three cases as listed in Table 1. For the proposed PON, the impacts of quantization bits and signal clipping on the BER performance are very similar to those reported in [15]. For fair transmission performance comparisons with the results presented in [14], in this paper, DAC/ADC quantization bits of 8 are chosen, which can be further reduced to approximately 5 without considerably degrading the optical back-to-back transmission performance [15]. From the parameters in Table 1, an identical upstream net bitrate of 6.25Gb/s can be calculated for each sub-band. As Hybrid Case-II(A) and Hybrid Case-II(B) support eight sub-bands, an aggregate upstream net signal bitrate of 50Gb/s is thus achievable, while for Hybrid Case-I, its supported four sub-bands result in an aggregate upstream net signal bitrate of 25Gb/s. To accommodate eight ONUs in the entire spectral region for the proposed PON, the minimum oversampling factor M is taken to be 8 [10]. In each ONU, an ideal intensity modulator (IM) is used to convert electrical to optical signal at a fixed optical launch power of 0dBm.

In the OLT, a variable optical attenuator (VOA) adjusts the received optical signal power and then a PIN with a quantum efficiency of 0.8 and a receiver sensitivity of -19dBm performs O-E conversion, followed by an ideal 15GHz electrical low pass filter to remove out-of-band noise. After the ADC, the DSP signal demodulation procedure illustrated in Fig. 2 is used to demodulate all received OFDM sub-bands for Hybrid Case-II(A) and Hybrid Case-II(B). For Hybrid Case-I, the DSP procedure is similar to that reported in [14], namely S/P conversion, 256-point FFT operation, sub-band identification process, optimum sideband selection process, conventional OFDM subcarrier equalization and decoding. Similar to the sideband identification described in Section 2, the subcarriers in each sub-band of a specific sub-wavelength are identified. For each identified OFDM signal, the corresponding sideband (LSB or USB) that suffers less channel fading is selected for signal recovery. For a 40km SSMF transmission distance, a system frequency response dip is observed at ~10GHz, as depicted in Fig. 4. The LSB in the 1st and 2nd sub-wavelengths and the USB in the 4th sub-wavelength are chosen for signal recovery for Hybrid Case-I. Signals occupying the 3rd sub-wavelength cannot be used to recover any information because of the channel fading effect.

4. Simulation Results

4.1 Upstream Transmission Performance

Using the parameters mentioned in Section 3, upstream transmission performances over 40km SSMF IMDD PON systems are modelled for the three cases and results are illustrated in Fig. 5. Channel 3 (CH3) for Hybrid Case-I and Channels 5 (CH5) and 6 (CH6) for both Hybrid Case-II(A) and Hybrid Case-II(B) are not operational due to channel fading as shown in Fig. 4. Consequently, their bit error ratio (BER) performances are not depicted in Fig. 5. In addition, back-to-back (B2B) BER performances of the operational channels at the lowest and highest frequencies for each
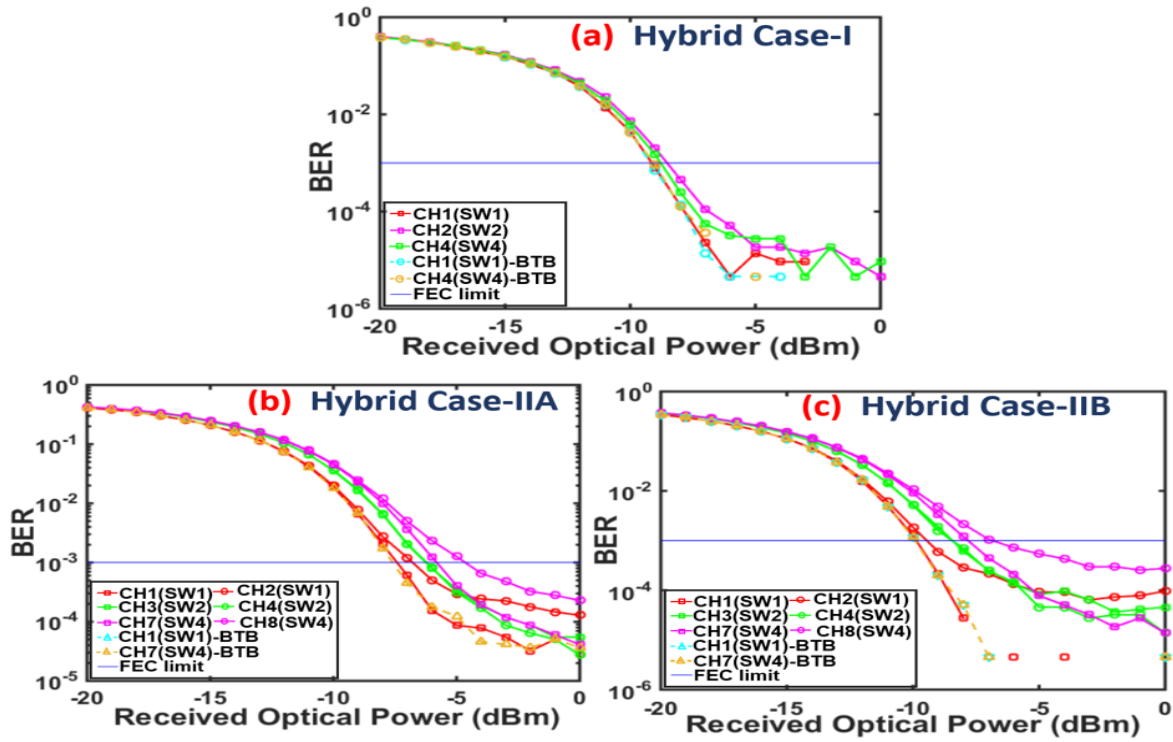
Fig. 5. BER performance versus received optical power after 40km SSMF IMDD PON transmission system subject to 0dBm optical launch power with channel bitrate of 6.25Gb/s; (a) Hybrid Case-I (b) Hybrid Case-IIA and (c) Hybrid Case-IIB. SW: sub-wavelength, CH: channel, BTB: back-to-back.
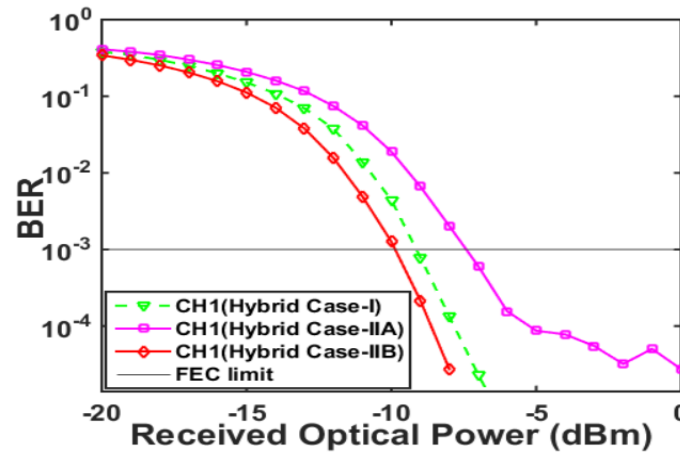

Fig. 6. Comparison of BER versus received optical power for all three involved cases after 40km SSMF IMDD PON transmission system for Channel-1.

case are also plotted to investigate nonlinear system impairment-induced upstream performance degradations.

In Fig. 5(a), the calculated BER performances show that for Hybrid Case-I, three channels can achieve BERs below the forward error correction (FEC) limit of 1.0×10^{-3}. As each channel has a net signal bit rate of 6.25Gb/s, the aggregate upstream net signal transmission capacity is 18.75Gb/s. For Hybrid Case-II(A) and Hybrid Case-II(B), as shown in 5(b) and 5(c) respectively, six of the channel BERs are below the FEC limit. This results in an aggregate upstream net signal bit rate of 37.5Gb/s. The proposed PON can thus lead to a higher spectral efficiency.

Fig. 5(b) and 5(c) also show that in comparison to Hybrid Case-I, relatively large receiver sensitivity variations are observed among different sub-bands for both Hybrid Case-II(A) and Hybrid Case-II(B). This is a result of channel fading which leads to undesirable power leakage between orthogonal sub-bands sharing a sub-wavelength spectral region [13], [18], [19]. However, no such power leakage occurs for Hybrid Case-I, as only an I-phase sub-band exists within each

individual sub-wavelength spectral region, as shown in Fig.3(a). These receiver sensitivity variations are not observed in the B2B transmission systems where the lowest frequency channel and highest frequency channel have almost identical BER performances for all three cases. It should be noted that the abovementioned imperfect orthogonality-induced power leakage between different channels can be significantly reduced when the cross-channel interference cancellation technique reported in [13], [18], [19] is used.

CH1 BER curves of the three cases shown in Fig. 5 are plotted in Fig. 6(a). It can be seen that Hybrid Case-II(A) has ~1.5dB receiver sensitivity degradations when compared to Hybrid Case-I. This is due to the fact that the overall ONU count in Hybrid Case-II(A) is double that of Hybrid Case-I. The higher ONU count gives rise to effective optical signal noise ratio (OSNR) reductions in each channel and leads to ~1.5dB receiver sensitivity degradations [20]. Hybrid Case-II(B) has an identical ONU number compared to Hybrid Case-I and a ~0.7dB improvement in receiver sensitivity compared to Hybrid Case-I. This is mainly attributed to an increase in effective OSNR arising from directly combining spectrum-sharing ONU sub-band signals in the digital domain [20].

Fig. 6 also shows that for the adopted numerical simulation parameters, for Hybrid Case-II (A) and Hybrid Case-II (B), their receiver sensitivities are -7.3dBm and -9.6dBm respectively, both of which can be further improved when use is made of some well-documented techniques such as wavelength-offset optical filtering [21] and DSP-enabled optical field reconstruction in the receiver [22].
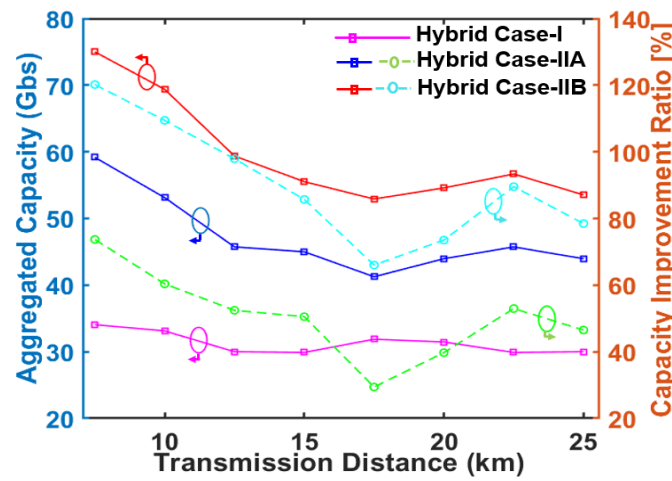

Fig. 7. Maximum aggregate upstream transmission capacity versus reach for IMDD PON system.
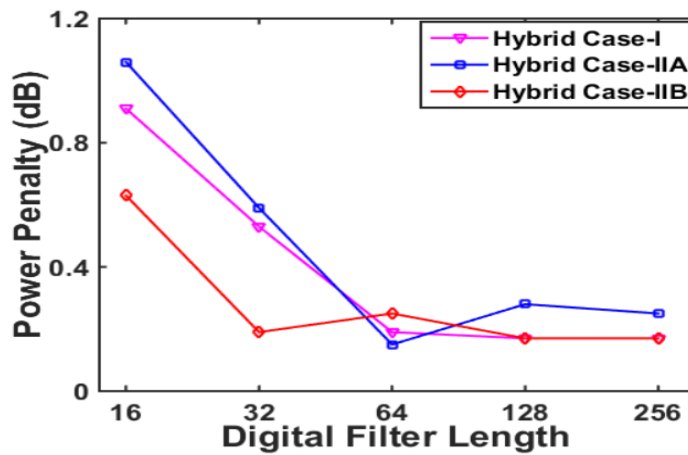

Fig. 8. Channel interference-induced power penalties for 40km upstream signal transmission for different IMDD PONs incorporating with various digital filter lengths.

4.2 Upstream Transmission Capacity versus Reach Performance

With the simulation parameters used to obtain Fig. 6, maximum achievable upstream net signal transmission capacities are explored as a function of fiber transmission distance, and corresponding results are plotted in Fig. 7. For these results, adaptive bit-loading is applied to all subcarriers involved in each OFDM signal with signal modulation formats varying from DBPSK,

DQPSK, 4/8/16/32/128-QAM to 256-QAM. The received optical powers (ROPs) are fixed at -5dBm. Signal capacity improvement ratios between Hybrid Case-II(A)/Hybrid Case-II(B) and Hybrid Case-I are plotted in the same figure.

In Fig. 7, it can be seen that across the transmission distance range of 50km, Hybrid Case-II(A) (Hybrid Case-II(B)) can improve the maximum aggregate upstream net signal transmission capacity by a factor of up to 1.7 (2.2) compared with Hybrid Case-I. Thus, the proposed PON improves the upstream transmission capacity. As expected from Fig.5 and Fig.6, Hybrid Case-II(B) can further improve the upstream signal transmission capacity with respect to Hybrid Case-II(A) because of digital-domain sub-band multiplexing-induced effective OSNR improvements, as discussed in Section 4.1.

4.3 Channel Interference Effect

As described in Section 2, digital orthogonal filtering plays a key role in the proposed PON. It is well known [10] that for a specific digital filter, a relatively short filter length can lead to a relatively large power leakage, resulting in undesirable channel interferences. However, a long filter increases the digital filter DSP complexity. Using the simulation parameters identical to those in Fig.5, the digital filter length-dependent channel interference-induced power penalties are investigated for all three cases. Results are presented in Fig. 8. Here the power penalty is defined as the difference of ROPs at the FEC limit with and without spectral spaces between adjacent channels of different sub-wavelengths. In calculating Fig. 8, 16-QAM signal modulation formats are adopted for all subcarriers in each involved OFDM signal, and fiber transmission distances are fixed at 40 km.

As seen in Fig. 8, <1.2dB (<0.8) power penalties are observed for Hybrid Case-II(A) (Hybrid Case-II(B)) when the proposed PONs employ digital filter lengths as short as 16. While for a digital filter length of 64 and beyond, <0.3dB power penalties can be observed for all the considered cases. Hybrid Case-II(A) suffers the highest power penalties when compared to Hybrid Case-I and Hybrid Case-II(B). This is mainly because Hybrid Case-II(A) suffers the strongest unwanted cross talk effect between two spectrally overlapped orthogonal sub-bands [18], [19]. It can also be seen from Fig. 8 that an optimum digital filter length of 64 results in acceptable channel interferences and has low digital filter DSP complexity.

5. Conclusions

By modifying the DSP algorithms implemented in the OLT and ONUs, a new IMDD hybrid OFDM-DFMA PON has been reported for the first time, where digital orthogonal filtering-based two spectrally overlapped sub-bands occupying an individual sub-wavelength spectral region carry independent ONU information for upstream transmission. A model of the proposed PON has been developed, and its upstream transmission performances for various application scenarios have been examined and compared with the previously reported PONs. It has been shown that the proposed PON maintains features associated with the previously reported PONs. Moreover, compared with the previously reported PON, the new PON supports twice as many ONUs passively multiplexed in the optical domain and allows >1.7-fold upstream transmission capacity increases with <1.5dB upstream power budget degradations. Under the condition of the same number of ONUs occupying two digitally multiplexed sub-bands in a single sub-wavelength spectral region, >0.7dB upstream power budget improvements and >2.2-fold upstream transmission capacity enhancements can be achieved. In addition, the proposed PONs have excellent tolerance to finite digital filter tap length-induced channel interferences.

Acknowledgements

References

[1] P. Chanclou, A. Cui, F. Geilhardt, H. Nakamura, and D. Nesset, "Network operator requirements for the next generation of optical access networks," IEEE Netw. Mag., vol. 26, Issue 2, pp. 8–14, 2012.

[2] X. Liu and F. Effenberger, "Emerging optical access network technologies for 5G wireless" J. Opt. Commun. Netw., vol. 8, no. 12, pp. B70–B79, 2016.

[3] 3GPP, "3rd generation partnership project; technical specification group radio access network; NG-RAN; architecture description (Release 15)," TS 38.401 V15.3.0, 2018.

[4] Y. Okumura and J. Terada, "Optical network technologies and architectures for backhaul/fronthaul of future radio access supporting big mobile data," Opt. Fibre Commun. Conf. (OFC), 2014.

[5] X. Liu and F. Effenberger, "Emerging optical access network technologies for 5G wireless," J. Opt. Commun. Netw., vol. 8, no. 12, pp. B70–B79, 2016.

[6] M. A. Habibi, M. Nasimi, B. Han and H. D. Schotten, "A Comprehensive Survey of RAN Architectures Toward 5G Mobile Communication System," IEEE Access, vol. 7, pp. 70371–70421, 2019.

[7] S. Chen and J. Zhao, "The requirements, challenges, and technologies for 5G of terrestrial mobile telecommunication," IEEE Commun. Mag, vol. 52, no. 5, pp. 36–43, 2014.

[8] C. I, Y. Yuan, J. Huang, S. Ma, C. Cui and R. Duan, "Rethink fronthaul for soft RAN," IEEE Commun. Mag., vol. 53, no. 9, pp. 82–88, 2015.

[9] M. Bolea, R. P. Giddings, M. Bouich, C. Aupetit-Berthelemot, and J. M. Tang, "Digital filter multiple access PONs with DSP-enabled software reconfigurability," J. Opt. Commun. Netw., vol. 7, no. 4, pp. 215–222, 2015.

[10] M. Bolea, R. P. Giddings, and J. M. Tang, "Digital orthogonal filter- enabled optical OFDM channel multiplexing for software-reconfigurable elastic PONs," J. Lightw. Technol., vol. 32, no. 6, pp. 1200–1206, 2014.

[11] X. Duan, R. P. Giddings, S. Mansoor, and J. M. Tang, "Experimental demonstration of upstream transmission in digital filter multiple access PONs with real-time reconfigurable optical network units," J. Opt. Commun. Netw., vol. 9, no. 1, pp. 45–52, 2017.

[12] M. L. Deng, A. Sankoh, R. P. Giddings, and J. M. Tang, "Experimental demonstrations of 30Gb/s/λ digital orthogonal filtering-multiplexed multiple channel transmissions over IMDD PON systems utilizing 10G- class optical devices," Opt. Express, vol. 25, no. 20, pp. 24251–24261, 2017.

[13] E. Al-Rawachy, R. P. Giddings, and J. M. Tang, "Experimental demonstration of a real-time digital filter multiple access PON with low complexity DSP-based interference cancellation," J. Lightw. Technol., vol. 37, no. 17, pp. 4315–4329, 2019.

[14] Y. X. Dong, R. P. Giddings, and J. M. Tang, "Hybrid OFDM-digital filter multiple access PONs," J. Lightw. Technol., vol. 36, no. 23, pp. 5640–5649, 2018.

[15] W. Jin, A. Sankoh, Y. X. Dong, Z. Q. Zhong, R. P. Giddings, M. O'Sullivan, J. Lee, T. Durrant and J. M. Tang., "Hybrid SSB OFDM-Digital filter multiple access PONs," J. Lightw. Technol., early access, Jan. 2020.

[16] X. Jin, R. P. Giddings, and J. M. Tang, "Real-time transmission of 3Gb/s 16-QAM encoded optical OFDM signals over 75km SMFs with negative power penalties," Opt. Express, vol. 17, pp. 14574-14585, 2009.

[17] Y. X. Dong, W. Jin, R. P. Giddings, M. O'Sullivan, A. Tipper, T. Durrant, and J. M. Tang, "Hybrid DFT-spread OFDM-digital filter multiple access PONs for converged 5G networks," J. Opt. Commun. Netw., vol. 11, no. 7, pp. 347–353, 2019.

[18] Y. X. Dong, E. Al-Rawachy, R. P. Giddings, W. Jin, D. Nesset, and J. M. Tang, "Multiple channel interference cancellation of digital filter multiple access PONs," J. Lightw. Technol., vol. 35, no. 1, pp 34–44, 2017.

[19] E. Al-Rawachy, R. P. Giddings, and J. M. Tang, "Experimental demonstration of a DSP-based cross-channel interference cancellation technique for application in digital filter multiple access PONs," Opt. Express, vol. 25, no. 4, pp. 3850–3862, 2017.

[20] X. Q. Jin, J. Groenewald, E. Hugues-Salas, R. P. Giddings, and J. M. Tang, "Upstream power budgets of IMDD optical OFDMA PONs incorporating RSOA intensity modulator-based colorless ONUs," J. Lightw. Technol., vol.31, no. 12, pp. 1914–1920, 2013.

[21] J. L. Wei, C. Sánchez, E. Hugues-Salas, P. S. Spencer and J. M. Tang, "Wavelength-offset filtering in optical OFDM IMDD systems using directly modulated DFB lasers," J. Lightw. Technol., vol.29, no.18, pp.2861-2870, 2011.

[22] H. Chen, N. K. Fontaine, J. M. Gene, R. Ryf, D. T. Neilson, and G. Raybon, "Dual polarization full-field signal waveform reconstruction using intensity only measurements for coherent communications," J. Lightw. Technol., vol. 38, no. 9, pp. 2587-2597, 2020.